16th World Conference on Earthquake, 16WCEE 2017

Santiago Chile, January 9th to 13th 2017

Paper N° XXXX (Abstract ID)

Registration Code: S-XXXXXXXX

NEW CYCLIC TENSILE MODEL FOR TWO-DIMENSIONAL FINITE ELEMENT ANALYSIS OF RC MEMBERS.

A. Kagermanov(1), P. Ceresa(2)

(1) PhD Candidate, UME School, Istituto Universitario di Studi Superiori, Pavia, 27100, Italy, alexander.kagermanov@umeschool.it
(2) Assistant Professor, UME School, Istituto Universitario di Studi Superiori, Pavia, 27100, Italy, paola.ceresa@iusspavia.it

Abstract

This paper presents a new approach for modeling the tensile cyclic response of reinforced concrete (RC) subjected to biaxial stress conditions. The model is based on equilibrium, constitutive and compatibility conditions applied on a cracked RC element with arbitrary reinforcement configuration. Cyclic bond degradation effects are accounted for in order to provide physical meaning to tension-stiffening, crack-closing and crack-opening phenomena. The proposed model was implemented into an orthotropic, smeared-crack membrane finite element based on the fixed-crack assumption. A number of verification examples on reinforced concrete panels, shear critical beams and walls subjected to monotonic and cyclic loading is presented. Emphasis is made on adequate modeling of shear failures, due to its detrimental effect on strength and energy dissipation capacity.

Keywords: reinforced concrete, cyclic analysis, membrane elements, shear, tensile behavior

1. Introduction

Two-dimensional reinforced concrete (RC) members, such as squat walls, beam-column joints and coupling beams play a crucial role in providing lateral strength and stiffness in building structures. However, they are prone to brittle failure modes if ductile behavior is not provided by adequate design and detailing. Of particular concern are existing RC structures located in seismic regions and designed before the introduction of capacity design principles and more rational member design approaches, such as those related to shear design.

Although significant improvements have been made in the recent seismic design codes to prevent brittle shear failures, deeper understanding of shear transfer mechanisms is required for an adequate assessment of member strength and ductility. Current design codes provide empirically based equations that may result in inaccurate and even unconservative predictions for members outside the dataset used for their calibration [8, 14, 17].

At the same time, significant effort has been made in developing analytical models for RC members in biaxial stress conditions capable of predicting brittle failure modes [4, 12, 18]. Implementation of these models within the Finite Element Method (FEM) allows modeling structural systems under more realistic loading and boundary conditions. Good agreement has been generally found with experimental tests of uniformly reinforced members subjected to monotonic loading [4, 19]. Although the monotonic response represents a good approximation to the envelope of the cyclic response, several response parameters associated to reversed cyclic loading cannot be directly obtained, such as residual deformations, hysteretic energy dissipation and cyclic stiffness and strength degradation. These parameters result to be of paramount importance in the framework of performance-based engineering.

Meanwhile, accuracy of analytical results under cyclic loading conditions is highly dependent on reliable constitutive models and robust numerical algorithms. Several experimental tests were conducted on cyclic behavior of RC panels and walls [10, 11, 13, 16], which helped refining and developing improved analytical models. However, different researchers developed different models for the same problem, whereas a general and unanimously accepted method is still lacking.

An attempt is made in the present work to provide a rational cyclic constitutive model for reinforced concrete in tension. The model is closely based on the mechanistic approach introduced in [15]. It uses equilibrium, compatibility and constitutive relations in the calculation of average concrete stresses at given tensile strains. Bond degradation effects are accounted for in a smeared way by means of the hysteretic bond model. The procedure is implemented in a two-dimensional membrane finite element using a single-crack fixed-crack approach. The level of agreement with experimental results for RC panels, walls and shear critical beams is finally discussed.

2. Analytical procedure

2.1 Proposed cyclic tensile model

Fig. 1 shows a cracked RC element with an average crack spacing s and a steel layer of reinforcement ratio ρ in the x direction. Total principal tensile strains ε_x are applied normal to the cracks, while ε_y are transverse strains causing Poisson expansion. Three regions can be distinguished in the element: (b) fully bonded, (sl) partially bonded and (cr) crack region.

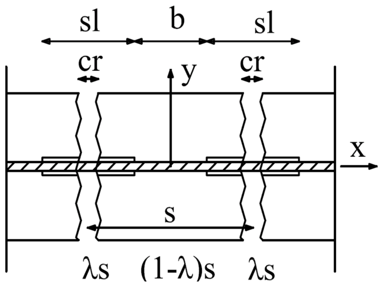

Fig. 1 – Cracked reinforced concrete element

The unbonded length parameter λ represents the partially bonded portion, where bond-slip occurs (So et al. 2008). Thus the total strain ε_x can be expressed as a function of λ and the local steel strains:

$$\varepsilon_x = (1\text{-}\lambda)\varepsilon^b{}_s + \lambda\,(\varepsilon^{sl}{}_s + \varepsilon^{cr}{}_s) \tag{1}$$

Alternatively Eq. (1) can be expressed as a function of concrete local strains [15]:

$$\varepsilon_x = (1\text{-}\lambda)\varepsilon^b{}_c + \lambda\,(\varepsilon^{sl}{}_c + \varepsilon^p{}_c + \varepsilon^{cr}{}_c) \tag{2}$$

Full compatibility of strains in (b) implies that $\varepsilon^b{}_c = \varepsilon^b{}_s = \varepsilon^b$. Concrete strains due to Poisson are given as $\varepsilon^p{}_c = -\nu\varepsilon_y$, where ν takes the value of 0.25 before yielding and 1.90 afterwards, based on the experimental work by [20]. Average concrete stresses are computed averaging concrete local stresses in the three regions (b), (sl) and (cr):

$$\sigma^{av}{}_c = \frac{(1-\lambda)s\sigma^b{}_c + (\lambda-\varepsilon_x)s\sigma^{sl}{}_c + \varepsilon_x s\sigma^{cr}{}_c}{s} \tag{3}$$

Since total strains ε_x are comparatively small, Eq. (3) can be simplified to:

$$\sigma^{av}{}_c = (1\text{-}\lambda)\sigma^b{}_c + \lambda\sigma^{sl}{}_c \tag{4}$$

Concrete crack stresses $\sigma^{cr}{}_c$ will be zero during opening of cracks, i.e. $-\varepsilon^{cr}{}_c > 0$. Upon unloading from tensile stresses, $\sigma^{cr}{}_c$ will be initially zero until closing of cracks ($\varepsilon^{cr}{}_c = 0$), after which compressive stresses will be transferred through contact between concrete blocks. In practice, contact might occur before complete closing of cracks due to misalignment of cracked surfaces. Analogously, average steel stresses are given as:

$$\sigma^{av}{}_s = (1\text{-}\lambda)\,\sigma^b{}_s + \lambda\sigma^{sl}{}_s \tag{5}$$

Local equilibrium conditions between two sections in the fully bonded (b) and bond slip regions (sl), and in the bond-slip (sl) and crack regions (cr) can be expressed as:

$$\sigma^b{}_c + \sigma^b{}_s = \sigma^{sl}{}_c + \sigma^{sl}{}_s \tag{6}$$
$$\sigma^{sl}{}_c + \sigma^{sl}{}_s = \sigma^{cr}{}_c + \sigma^{cr}{}_s \tag{7}$$

where steel stresses in the crack region $\sigma^{cr}{}_s$ have been introduced. Linear elastic constitutive relationships are valid for both steel and concrete in the fully bonded region. Thus it can be written:

$$\sigma^b{}_c = E_c\,\varepsilon^b{}_c \tag{8}$$
$$\sigma^b{}_s = \rho\,E_s\,\varepsilon^b{}_s \tag{9}$$

An elastic-perfectly plastic model is assumed for steel in (sl) and (cr) regions:

$$\sigma^{sl}_{s} = \rho\, E_s\, (\varepsilon^{sl}_{s} - \varepsilon^{sl}_{spl}) \leq \rho f_y \tag{10}$$
$$\sigma^{cr}_{s} = \rho\, E_s\, (\varepsilon^{cr}_{s} - \varepsilon^{cr}_{spl}) \leq \rho f_y \tag{11}$$

These strains are related to the average plastic strain as follows:

$$\varepsilon^{av}_{spl} = \lambda(\varepsilon^{sl}_{spl} + \varepsilon^{cr}_{spl}) \tag{12}$$

since plastic strains in the fully-bonded region are zero.

In the bond slip region, shear stresses will be transferred between steel and concrete inducing tensile stresses in the concrete. Assuming a constant distribution of shear stresses over the bond-slip length λs, the corresponding concrete force and stress are given as:

$$f^{sl}_{c} = \int_0^{\lambda x} \tau\pi\phi\, dx = \tau\pi\phi\lambda s \tag{13}$$

$$\sigma^{sl}_{c} = \frac{f^{sl}_{c}}{A_c} = \frac{\tau\pi\phi\lambda s}{A_c} = \tau 4 \frac{\rho}{\phi} \lambda s \tag{14}$$

In (14) bond stresses τ need to be evaluated. These are taken as a function of the total strain in the direction of the reinforcement $\tau(\varepsilon_x)$. Details on the proposed hysteretic function for $\tau(\varepsilon_x)$ can be found elsewhere [7].

The developments presented so far lead to seven unknown variables, which are: λ, σ^{av}_{c}, σ^{cr}_{s}, σ^{sl}_{s}, ε^{b}_{c}, ε^{sl}_{s} and ε^{cr}_{s}. Upon making use of the constitutive relations, the number of available equations is six: two average equilibrium (4) and (5), two local equilibrium (6) and (7), and two compatibility equations (1) and (2). Explicit calculation of ε^{sl}_{spl}, ε^{cr}_{spl} is not required, hence (12) is not included in the set of equations. In order to find a mathematical solution, it is assumed that ε^{b}_{c} is approximately 2 times the cracking strain. This allows calculation of the rest of variables and, in particular, of σ^{av}_{c}, which is used in the finite element calculations. Detailed description on the solution procedure is given in [7].

2.2 Compressive cyclic model

The tensile cyclic model presented so far is combined with a cyclic compressive model described below Fig. 2.

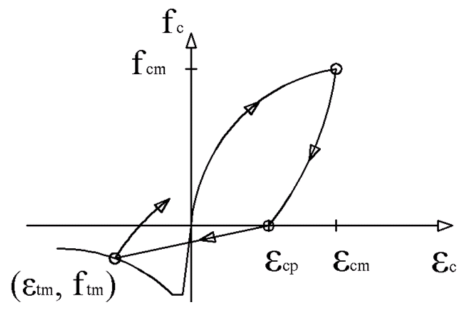

Fig. 2 – Combined compressive and tensile cyclic model

The compressive envelope is described by the Hognestad parabola with a reduction of the compressive strength due to simultaneous transverse tensile strains [18]:

$$\beta_\sigma = \frac{1}{0.80 - 0.34\varepsilon_{c2}/\varepsilon_o} \tag{15}$$

Nonlinear unloading follows the model from [12] with the plastic compressive strain given as:

$$\varepsilon_{cp} = \varepsilon_{c1} - \varepsilon_o \left(0.87(\varepsilon_{c1}/\varepsilon_o) - 0.166(\varepsilon_{c1}/\varepsilon_o)^2\right) \tag{16}$$

Cyclic strength and stiffness degradation is accounted for in the degradation parameter β_d:

$$\beta_d = \frac{1}{1+0.1\left((\varepsilon_{cm} - \varepsilon_{re})/\varepsilon_o\right)^{0.5}} \quad \text{for } \varepsilon_{cm} \leq \varepsilon_o$$

$$\beta_d = \frac{1}{1+0.175\left((\varepsilon_{cm} - \varepsilon_{re})/\varepsilon_o\right)^{0.6}} \quad \text{for } \varepsilon_{cm} \leq \varepsilon_o \tag{17}$$

Transition towards tensile strains is done linearly connecting the plastic strain ε_{cp} with the previous unloading point from the tensile envelope as shown in Fig. 2.

2.3 Shear stiffness

The shear stiffness of cracked reinforced concrete is modeled using the smeared shear stiffness approach for fixed-crack formulations, allowing divergence between principal stress and strain directions:

$$G = \frac{(\sigma_1 - \sigma_2)(\sin\Delta\theta_\sigma \cos\Delta\theta_\sigma)}{2(\varepsilon_1 - \varepsilon_2)(\sin\Delta\theta_\varepsilon \cos\Delta\theta_\varepsilon)} \tag{18}$$

Shear stresses at the crack arising from non-coincidence between principal directions and crack directions are calculated according to:

$$\tau = G\gamma \leq v_{ci,max} \tag{19}$$

An upper limit is set on the maximum interface shear transferred along cracks due aggregate interlock according to [18]:

$$v_{ci,max} = \frac{0.18\sqrt{f'_c}}{0.31 + \dfrac{24w}{16 + a_g}} \tag{20}$$

where w is the crack width and a_g the maximum aggregate size.

2.4 Uniaxial steel model

Average steel stresses and strains in equations (12) and (5) are determined using a uniaxial model for a mild steel bar embedded in concrete. The Menegotto-Pinto hysteretic model with modified isotropic hardening [6] is used. The average yield stress f_y^{av} of the embedded bar is determined according to [2]:

$$f_y^{av} = (0.91\text{-}2B)\, f_y$$

$$B = \frac{1}{\rho}\left(\frac{f_{ct}}{f_y}\right)^{1.5} \tag{17}$$

where f_{ct} is the concrete tensile strength, assumed to be $f_{ct} = 0.65(f'_c)^{0.33}$.

3. Finite Element Formulation

The material model described above was implemented within a small-strain membrane finite element. The element presents four nodes with three degrees of freedom (dofs) each: two translational and one rotational. This permits using higher-order displacement interpolation functions, resulting in relatively coarse meshes when compared with constant strain elements. Complete details on the element formulation are given elsewhere [7].

In order to account for material nonlinearity and solve the nonlinear system of equations, standard FEM procedures were used, such as the Newton-Raphson method with displacement control [1, 5]. The vector of internal total stresses $\boldsymbol{\sigma}_{xy}$ and the material stiffness matrix $\mathbf{D}_{xy}$, calculated at each integration point using the previously described constitutive models, are used to compute the vector of internal forces $\mathbf{F}_{int}$ and the tangent stiffness matrix $\mathbf{K}_T$ of the entire structure. A displacement-based convergence criteria is performed at each iteration step and, if not satisfied, a new estimate of incremental nodal displacements is calculated using $\mathbf{K}_T$ and the unbalanced force vector $\mathbf{R}$. New total strains are then computed using the strain-displacement $\mathbf{B}$ matrix. A summary is shown in the flow chart below Fig. 3.

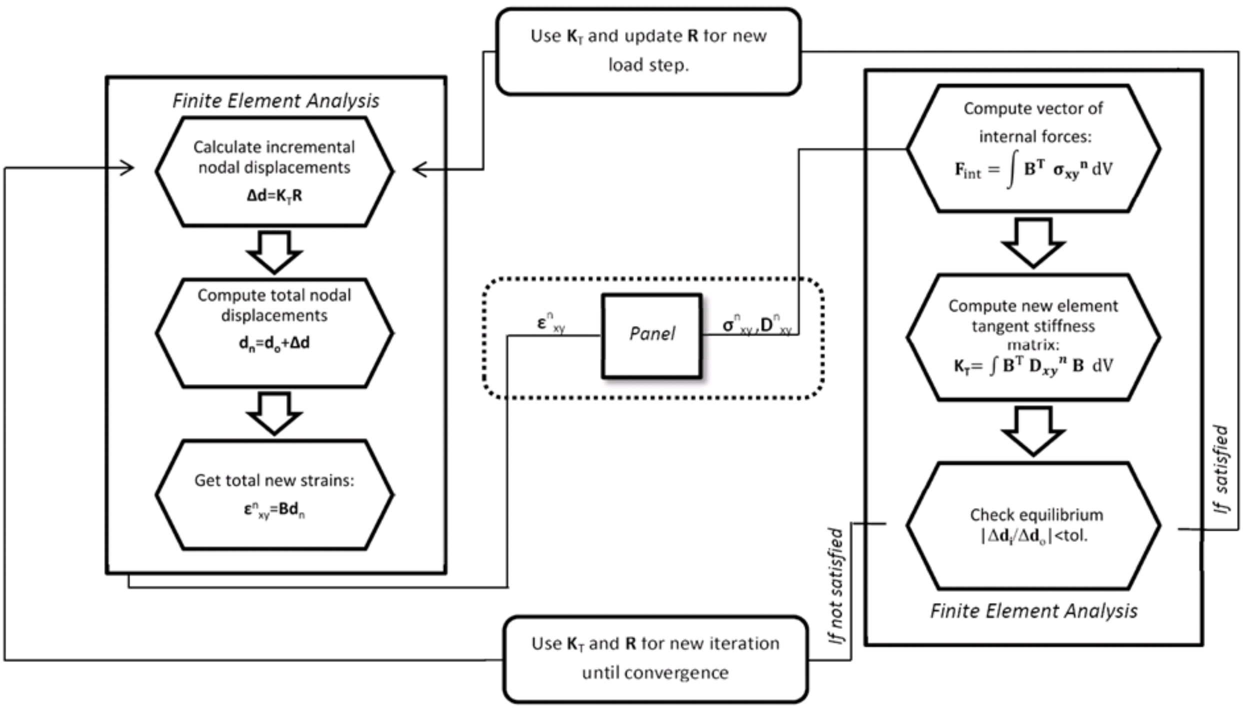

Fig. 3 – Flow chart on the FEM procedure

4. Numerical validation

4.1 RC panels

The series of SE panels tested by Stevens et al. (1991) were used for validation. It consisted of three square specimens 1524mm × 1524mm × 285mm subjected to pure cyclic shear and shear combined with biaxial compression Fig. 4. Specimen properties are summarized in Table 1. Calculations were done with an average crack spacing of 50mm, and a maximum bond stress of 5 MPa.

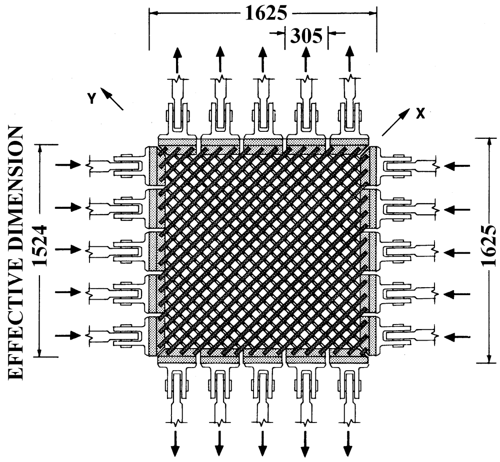

Fig. 4 – Panel test set up [16]

Table 1 – Panel material and loading properties.

Panel	Loading	Concrete		x- steel		y-steel	
	$(\sigma_x:\sigma_y:\tau_{xy})$	$\varepsilon_o(10^{-3})$	f_c'(MPa)	ρ_x(%)	f_{xy}(MPa)	ρ_y(%)	f_{yy}(MPa)
SE8	0:0:1	2.60	37.0	2.93	492	0.98	479
SE9	0:0:1	2.65	44.2	2.93	422	2.93	422
SE10	0.33:0.33:1	2.20	34.0	2.93	422	0.98	479

Fig.5 compares shear stress-strain results for panel SE9, which had equal reinforcement in both directions. This panel failed at a shear stress τ_{xy} = 9.55 MPa, after yielding of y-reinforcement. Under ideal laboratory conditions, panel SE9 should have failed upon simultaneous yielding of both x and y reinforcements at a theoretical value of 12.66 MPa [12]. The analytical value is 11.02 MPa which is closer to the theoretical one.

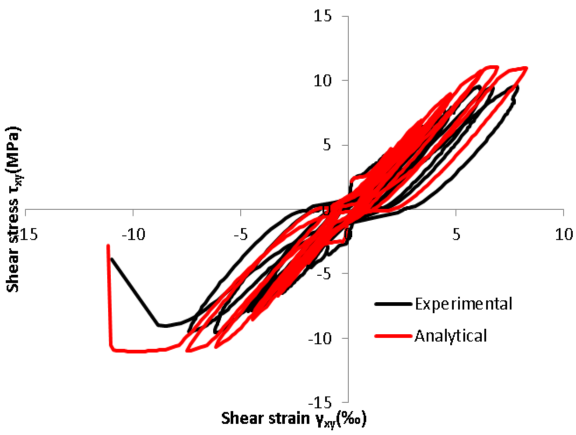

Fig. 5 – Shear stress-strain response for panel SE9

Fig.6 and Fig.7 compare shear stress-strain results for panels SE8 and SE10. Panel SE8 failed at 5.76 MPa due to concrete shear failure, after sustaining a large number of repeated cycles beyond yield, causing large permanent strains. Analytical results agree well with overall panel behavior, including hysteretic pinching and plastic strain accumulation. However, maximum shear stresses tend to be higher than the experimental ones in the post-yield range. Panel SE10 was subjected to combined shear and biaxial compression. It failed due to concrete crushing upon yielding of y-reinforcement. Very good agreement was found for this panel in terms of shear strength and hysteretic response.

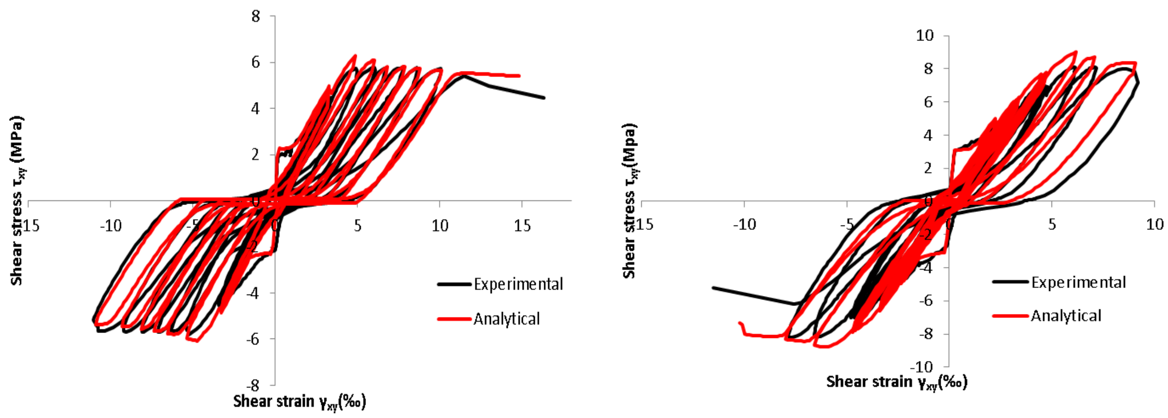

Fig. 6 – Shear stress-strain response for panel SE8 (left) and panel SE10 (right)

4.2 PCA walls

The series of Portland Cement Association (PCA) walls were tested in 1971 by Oesterle et al. [11] as part of an extensive experimental campaign on cyclic response of RC shear walls. Specimens B2 and B8 were selected for analysis. Both walls were 4570mm × 1910mm specimens with 305mm thick flanges and 102mm thick web (Fig.7). The main difference was the presence of confining steel in the boundary zone (ρ_y=1.35% with f_y=455MPa) and an applied constant axial stress of 3.75MPa for wall B8 (Table 2). Both walls were built integral with a heavy base structure and stiff top slab, at which cyclic lateral displacements were applied in 25mm increments with two excursions at each.

Table 2 – PCA wall material and loading properties.

Wall zone	Tickness	Concrete		x-steel		y-steel	
	t(mm)	E_c(MPa)	f_c'(MPa)	ρ_x(%)	f_{xy}(MPa)	ρ_y(%)	f_{yy}(MPa)
B2-Web	102	32700	53.7	0.63	533	0.29	533
B2-Flanges	305	32700	53.7	0.63	533	3.67	410
B8-Web	102	25600	42.1	1.38	489	0.29	455
B8-Flanges	305	25600	42.1	1.38	489	3.67	448

The FE mesh is shown in Fig.7. A total of 28 elements, with 2 × 2 integration points (IPs) each, were used to model the web and flanges, while 4 were used to model the top slab. Fixed boundary conditions were assumed at the bottom wall elements. The lateral displacement was imposed at the top left corner, using the corresponding horizontal degree of freedom as displacement control. Vertical forces were applied at the top slab for specimen B8, in order to simulate the effect of constant axial load. The tensile concrete model was defined with an average crack spacing of 50mm, maximum bond stress of 5MPa.

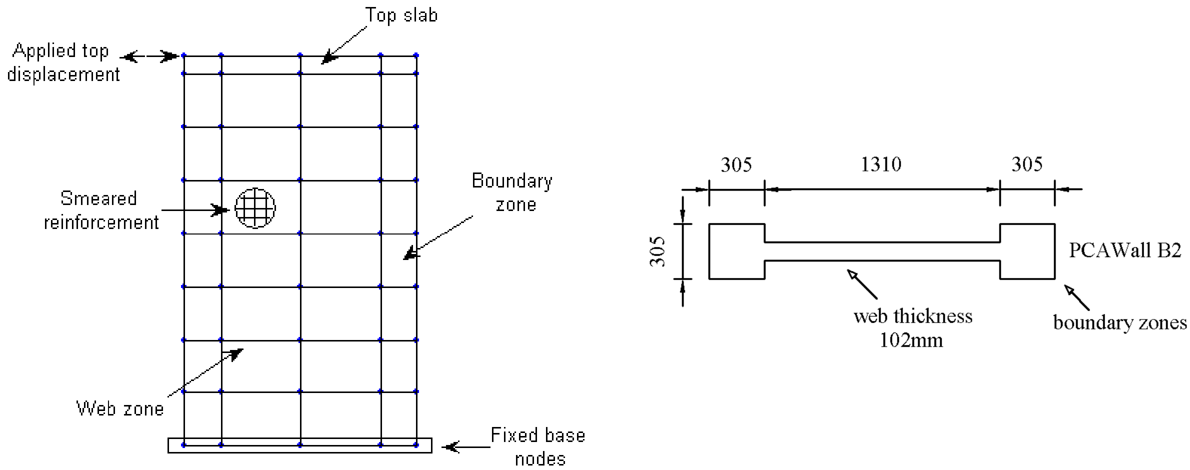

Fig. 7 – PCA Walls mesh and cross section (in mm)

The hysteretic lateral force-displacement response is compared in Fig. 8. Good agreement is found for wall B8, while some shortcomings can be identified for wall B2. For instance, initial stiffness and strength is significantly overestimated. It was found from the experimental program [11] that wall B2 had been subjected to previous load cycles below yield which pre-cracked the wall. Relatively good agreement is observed in terms of cyclic strength and unloading stiffness, whereas hysteretic pinching is overestimated, especially at positive displacements. The axial load in wall B8 increases stresses normal to crack, thus decreasing shear slip and hysteretic pinching. Also, existence of confining steel causes larger axial strains in the boundary zones when compared to diagonal stresses in the web, resulting in flexure-dominated type of resisting mechanism.

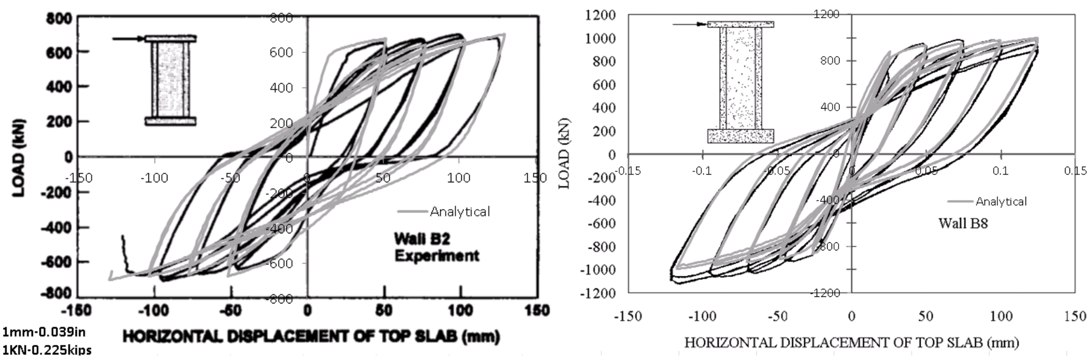

Fig. 8 –Lateral force-displacement response for PCA walls (adapted from Palermo 2003)

4.3 SW walls

SE walls were 600mm × 1200mm × 60mm rectangular specimens tested by Pilakoutas and Elnashai (1995). Walls SW4 and SW5 were selected for analysis. These walls had heavily reinforced boundary zones of varying length, mainly 110mm and 60mm for wall SW4 and SW5, respectively. Confining steel in form of rectangular hoops and cross ties was provided in the boundary regions for both specimens (Table 3). Due to the significant amount of flexural reinforcement in the boundary zones and the orthogonality of the cracks with respect to the latter, the average yield strength reduction as proposed by [2] was not applied.

Table 3 – PCA wall material and loading properties.

Wall zone	Tickness	Concrete		x-steel		y-steel	
	t(mm)	E_c(MPa)	f_c'(MPa)	ρ_x(%)	f_{xy}(MPa)	ρ_y(%)	f_{yy}(MPa)
SW4-Web	60	35240	37.0	0.39	545	0.50	545
SW4-Flanges	60	35240	37.0	0.79	545	6.86	470
SW5-Web	60	27820	31.8	0.31	400	0.59	545
SW5-Flanges	60	27820	31.8	0.31/0.66*	400	12.5	535

*In the bottom half of the boundary element

The FE mesh consisted of 60 2 × 2 IP membrane elements, with 12 elements in each flange and 48 in the web region (Fig. 9). The top slab was modelled with 9 elements, while fixed boundary conditions were assumed at the bottom elements. The tensile concrete model was defined with the same parameters as for the PCA walls. In addition, in order to simulate the effect of confinement, the monotonic compressive envelope was modified to the Popovics envelope with a confinement factor of 1.5 for SW5 [9].

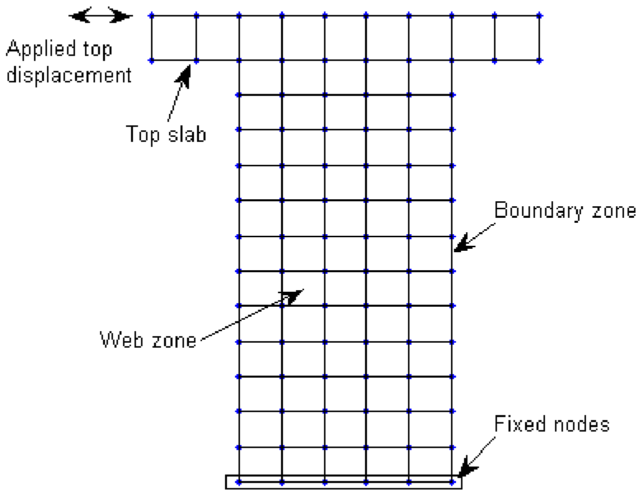

Fig. 9 – SW Walls mesh

Lateral force-displacement loops are compared in Fig.10. The response for wall SW4 is characterized by yielding of flexural reinforcement, with several inelastic excursions beyond yield without significant loss of strength and stiffness. Wall SW5 experienced extensive crushing of concrete in the bottom elements, both in the boundary and web zones, with subsequent cycles beyond the peak compressive strain causing significant strength and stiffness degradation. Analytical results are in relatively good agreement, capturing overall strength, permanent displacements and hysteretic stiffness and strength degradation, although some underestimation of strength in the post-peak range can be observed.

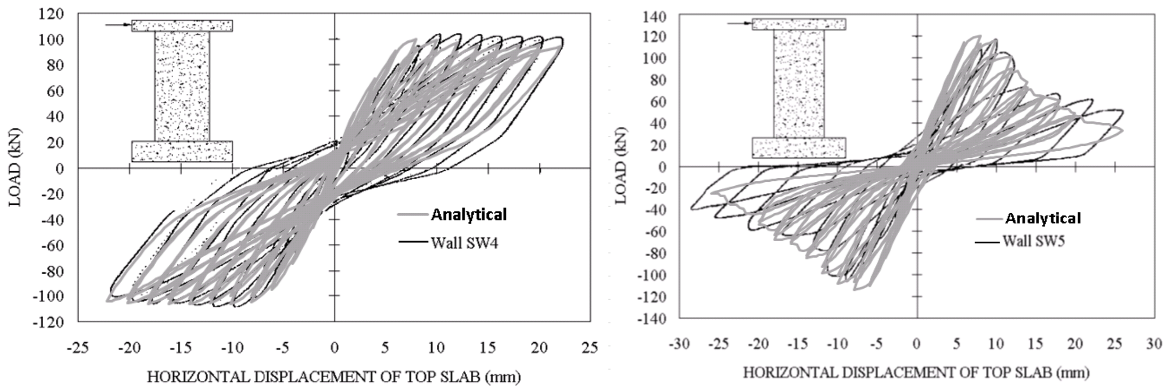

Fig. 10 – Lateral force-displacement response for SW walls (adapted from Palermo 2003)

4.4 Shear critical beams

A set of 12 RC beams were tested by Bresler and Scordelis [3] in order to investigate shear failure of members with different levels of longitudinal and transverse reinforcement. All beams were simply supported and monotonically loaded at mid- span under force control. The distance between supports varied between 3660mm and 6400mm, while the beam depth was kept constant and equal to 552mm (Fig. 11). Bottom longitudinal reinforcement was provided for all specimens, while only some of the beams contained top longitudinal reinforcement and transverse shear reinforcement. All beams failed in brittle manner due to shear in the web region.

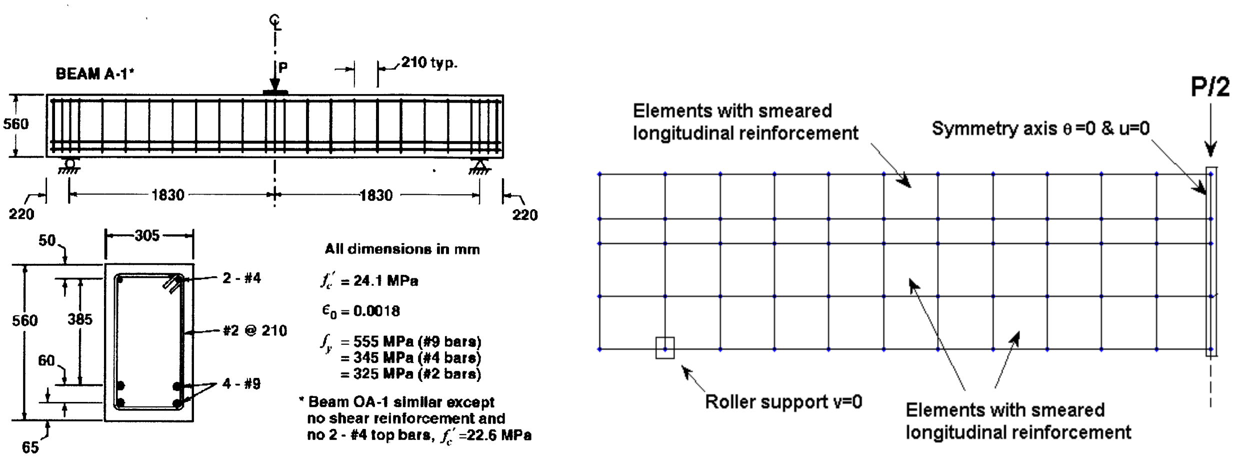

Fig. 11 – Beam properties.

Beams OA-1 and A-1 were selected for verification purposes. Tables 7 and 8 summarize beam properties and Fig. 12 shows the FE mesh configuration. Only half of the beam was modeled making use of symmetry conditions. The longitudinal reinforcement was smeared along a distance of 7.5 times the bar diameter in both directions, according to CEB-FIB. This resulted in some web elements in beam OA1 with no reinforcement at all.

Table 4 – Beam material and loading properties.

Beam	Width	Concrete		Reinforcement		
	b(mm)	$\varepsilon_o(10^{-3})$	f_c'(MPa)	Bottom	Top	Stirrups
OA1	305	1.8	22.6	4ϕ28	-	-
A1	305	1.8	24.1	4ϕ28	2ϕ12	ϕ6/210

Fig. 12 compares the monotonic force-displacement response at mid-span. Also predictions using the Modified Compression Field Theory, reported in [19], are included. The experiment was done under force-control, hence only the pre-peak behavior was measured. The analysis agrees relatively well in terms of initial stiffness, peak load and maximum displacement for beam A1. For beam OA1 (with no shear reinforcement), some divergence can be noted in terms of post-cracking stiffness and maximum displacement. Failure was localized in the unreinforced web elements due to shear slip along the diagonal cracks.

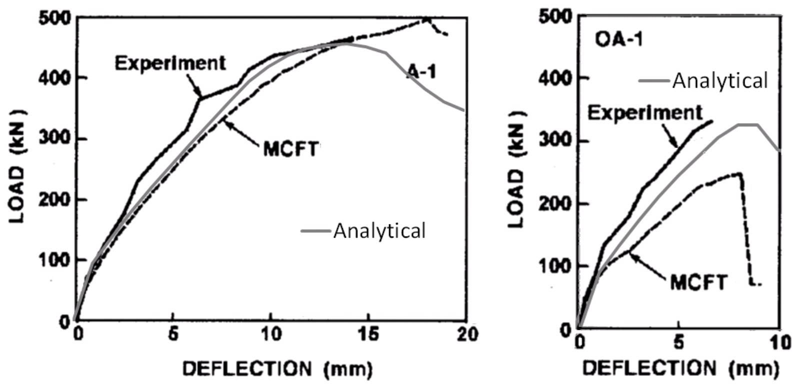

Fig. 12 – Force-displacement response for beam A-1 and OA1 (adapted from [19])

5. Conclusions

An analytical constitutive model for reinforced concrete in the tensile strain domain was presented. The model formulation followed the principles of mechanics, such as equilibrium, compatibility and constitutive relations. It was implemented into a membrane finite element and verified against a number of monotonic and cyclic tests on RC panels, shear critical beams and walls with aspect ratios less than 3. Promising results were obtained, even for beams with no shear reinforcement. Nevertheless, further verifications on more complex geometries and reinforcement configurations will be object of future research.

6. Acknowledgements

The authors are very grateful to Prof. M. P. Collins for providing raw experimental data from reversed-cyclic membrane SE-element tests conducted at the University of Toronto. The authors also acknowledge the constructive criticism of two anonymous reviewers, who certainly have contributed to an improvement of the quality of the manuscript.

5. References

[1] Bathe KJ (1996): *Finite Elements Procedures*. Prentice Hall, Inc., Upper Saddle River, New Jersey 07458.

[2] Belarbi A, Hsu TTC (1994): Constitutive Laws of Concrete in Tension and Reinforcing Bars Stiffened by Concrete, *ACI Structural Journal*, **91º(**4), 465-474.

[3] Bresler B, Scordelis AC (1963): Shear strength of RC beams, *ACI Journal Proceedings*, **60**º(1), 51-74.

[4] Cervenka V (1970): Inelastic Finite Element Analysis of Reinforced Concrete Panels under In-plane Loads. *Phd thesis*, University of Colorado, Boulder, Colorado.

[5] Crisfield M (1981): A fast incremental/iterative solution procedure that handles 'snap through', *Computers & Structures*, **13** (1-3), 55-62.

[6] Filippou FC, Popov EG, Bertero VV (1983): Effects of bond deterioration on hysteretic behavior of reinforced concrete joints, *Report No. UCB/EERC–83/19*, EERC. University of California, Berkeley.

[7] Kagermanov A (2015): Physically-based cyclic tensile model for RC membrane elements, *Individual Study*, UME School, IUSS, Pavia, Italy.

[8] Kim SJ, Elnashai A (2008): Seismic assessment of RC structures considering vertical ground motion. *Mid America Earthquake Center*. Report Nº 08-03.

[9] Mander JB, Priestley MJN, Park R (1988): Theoretical stress-strain model for confined concrete, *Journal of Structural Engineering,* **114**º(12), 1804-1826.

[10] Mansour M, Hsu TTC (2005): Behavior of Reinforced Concrete Elements under Cyclic Shear I: Experiments*, Journal of Structural Engineering,* ASCE, **131**º(1), 44-53.

[11] Oesterle RG, Fiorato AE, Johal LS, Carpenter JE, Russell HG, Corley WG (1976): Earthquake-Resistant Structural Walls-Tests of Isolated Walls, *Report to National Science Foundation, Construction Technology Laboratories*, Portland Cement Association, Skokie, III, 315.

[12] Palermo D, Vecchio FJ (2002): Behavior and Analysis of Reinforced Concrete Walls subjected to Reversed Cyclic Loading, *Publications No. 2002-01*, Department of Civil Engineering, University of Toronto, Toronto, Canada

[13] Pilakoutas K, Elnashai A. (1995): Cyclic Behavior of Reinforced Concrete Cantilever Walls, Part I: Experimental Results, *ACI Structural Journal*, **92**º(3), 271-281

[14] Priestley MJN, Verma R, Xiao Y (1994): Seismic shear strength of RC columns. *Journal of Structural Engineering,* **120**º(8), 2310-2329.

[15] So M (2008): Total Strain Based Bond/Slip And Shear/Friction Membrane Model For Finite Element Analysis Of Reinforced Concrete, *PhD Thesis*, University of Washington in St. Louis, St. Louis, Missouri

[16] Stevens NJ, Uzumeri SM, Collins MP (1991): Reinforced concrete subjected to reversed cyclic shear-experiments and constitutive models. *ACI Structural Journal*, **88**º(2), 135-146.

[17] Vecchio F, Collins M (1988): Predicting the response of RC beams subjected to shear using Modified Compression Field Theory. *ACI Structural Journal*. Title nº 85-S27, May-June

[18] Vecchio F, Collins M (1986): The Modified Compression Field Theory for RC elements subjected to shear. *ACI Journal*. Title nº 82-S22, January-February

[19] Vecchio F (2000): Analysis of shear critical reinforced concrete beams. *ACI Structural Journal*. Title nº 97-S12, January-February

[20] Zhu RRH, Hsu TTC (2002): Poisson Effect in Reinforced Concrete Membrane Elements, *ACI Structural Journal*, **99**º(5), 631-640.

[21] Zhu RRH, Hsu TTC, Lee JY (2001): Rational Shear Modulus for Smeared-Crack Analysis of Reinforced Concrete, *ACI Structural Journal*, **98**º(4), 443-450.